

Confinement and scaling in deep inelastic scattering

S. A. Gurvitz

Department of Particle Physics, Weizmann Institute of Science, Rehovot 76100, Israel

and TRIUMF, Vancouver, B.C., Canada V6T 2A3

Abstract

We show that parton confinement in the final state generates large $1/Q^2$ corrections to Bjorken scaling, thus leaving less room for the logarithmic corrections. In particular, the x -scaling violations at large x are entirely described in terms of power corrections. For treatment of these non-perturbative effects, we derive a new expansion in powers of $1/Q^2$ for the structure function that is free of infra-red singularities and which reduces corrections to the leading term. The leading term represents scattering from an off-mass-shell parton, which keeps the same virtual mass in the final state. It is found that this quasi-free term is a function of a new variable \bar{x} , which coincides with the Bjorken variable x for $Q^2 \rightarrow \infty$. The two variables are very different, however, at finite Q^2 . In particular, the variable \bar{x} depends on the invariant mass of the spectator particles. Analysis of the data at large x shows excellent scaling in the variable \bar{x} , and determines the value of the diquark mass to be close to zero. \bar{x} -scaling allows us to extract the structure function near the elastic threshold. It is found to behave as $F_2 \sim (1-x)^{3.7}$. Predictions for the structure functions based on \bar{x} -scaling are made.

11.10.St, 12.38.Lg, 13.60.Hb

Typeset using REVTeX

I. INTRODUCTION

Consider the inclusive scattering of a high energy electron, $e + N \rightarrow e' + X$, from a nucleon of mass M . The spacelike 4-momentum transferred to the target is $q = (\nu, \mathbf{q})$. For an unpolarized target the double-differential cross-section is determined by two structure functions $W_1(Q^2, \nu)$ and $W_2(Q^2, \nu)$ (or $F_1 = MW_1$, $F_2 = \nu W_2$), where $Q^2 = \mathbf{q}^2 - \nu^2$. These structure functions are given by the imaginary part of the forward Compton amplitude of the virtual photon with 4-momentum q (Fig. 1), where the nucleon vertex Γ is shown in Fig. 2. The first diagram in Fig. 1 corresponds to the Impulse Approximation (IA), and the second diagram describes the Final State Interaction (FSI) of a struck quark with spectator quarks and gluons (these are shown explicitly in Fig. 2). The IA term is expected to become dominant in the structure function for $Q^2 \gtrsim 10$ (GeV/c)². As a result F_1 and F_2 turn out to be functions of the Bjorken variable $x = Q^2/2M\nu$, i.e. $F_i(x, Q^2) \rightarrow F_i(x)$, where $F_i(x)$ is directly related to the parton distribution $\tilde{q}(x)$ (the Bjorken scaling), as for instance

$$\nu W_2(Q^2, \nu) = F_2(x, Q^2) \rightarrow \sum_i e_i^2 x \tilde{q}_i(x). \quad (1.1)$$

The existing data in fact, show considerable Q^2 -dependence of the structure functions, as for the proton structure function from the BCDMS [1] and SLAC [2] experiments shown in Fig. 3. (The solid lines correspond to a 15 parameter fit [3]). Usually the scaling deviation of the structure functions is attributed mainly to the logarithmic corrections from gluon radiation, which is contained in the first diagram in Fig. 1 [4]. Corrections $\sim 1/Q^2$ arising from the second diagram in Fig. 1 (higher twist terms) are usually considered as playing a minor role in scaling violation, even at moderate Q^2 .

This common disregard of the FSI terms for $Q^2 \gtrsim 10$ (GeV/c)² is very surprising, especially in view of parton confinement. At first sight, the confining interaction of partons in the final state should influence the structure function strongly. Consider for instance the example of two *nonrelativistic* “quarks” of mass m interacting via a harmonic oscillator potential [5]. These quarks are never free and therefore the system in the final state possesses

a discrete spectrum. As a result the structure function, $F(q, \nu)$, as a function of ν , is given by a sum of δ - functions. Obviously, it looks very different from the structure function obtained in the IA, which considers the struck parton as a free particle in the final state. This paradox can be resolved by introducing a scaling variable y [6]

$$y = -\frac{|\mathbf{q}|}{2} + \frac{m\nu}{|\mathbf{q}|}, \quad (1.2)$$

where $(m - y)/M$ is a non-relativistic analogue of the Bjorken variable x . Then expanding the structure function $\mathcal{F}(q, y) \equiv F(q, \nu)$ in powers of $1/q$, one finds in the limit $q \rightarrow \infty$ and $y = \text{const}$ that it becomes a smooth curve, $\mathcal{F}(q, y) \rightarrow \mathcal{F}_0(y)$, which coincides with a free parton response [5,7]. Although this result appears to confirm the parton model picture, it does not imply that the interaction in the final state is not important. The latter has been merely incorporated in $\mathcal{F}_0(y)$ by an appropriate choice of the scaling variable y , which diminishes the contribution from higher-order ($\sim 1/q$) correction terms. For instance, a different choice of the scaling variable could result in very large or even singular corrections to the structure function.

It is practically impossible to calculate the structure function including FSI, except for a few simple nonrelativistic models [5,7]. Therefore it is very important to find an optimal expansion of the structure function of confined systems, which reduces higher order corrections ($\sim 1/q$) to the zero order (quasi-free) term. For a non-relativistic case such an expansion, which leads to the scaling variable y , Eq. (1.2), was proposed by Gersch, Rodriguez and Smith [8]. (This expansion was designed for weakly bound systems, but appears in fact to be applicable to confined systems as well [7]). Unfortunately, the situation in the relativistic case looks very different, and no simple extrapolation of the non-relativistic results seems to be possible.

In this paper we attempt an optimal expansion for the *relativistic* structure function, that can be applied to confined systems, i.e., it is free of infra-red singularities, and diminishes the contribution from FSI. Then the zero order (quasi-free) term effectively incorporates effects of *confining* FSI, and thus can be considered a good approximation for the structure

function, valid also for *nonasymptotic* Q^2 . Such a quasi-free approximation leads to scaling of the structure function in a new scaling variable. Finally, we perform the analysis of data in terms of this scaling variable and compare the results with a standard approach.

The plan is as follows: A relativistic expansion of the structure function in powers of $1/Q^2$ is derived in Section 2. It is shown that infra-red singularities generated by confining FSI are eliminated. The leading, quasi-free term is discussed in Section 3. We demonstrate there that the structure function is a function of a new scaling variable. The evaluation of the first correction term for the linear-rising potential is presented in Section 4. An analysis of data and predictions for new experiments are given in Section 5. The last Section is summary.

II. RELATIVISTIC STRUCTURE FUNCTION

Consider the nucleon structure function W given by the imaginary part of the forward Compton amplitude, Fig. 1. For the sake of simplicity we take all the constituents and the virtual photon as scalar particles. Here $P = (M, 0)$ is the 4-momentum of a target (in the laboratory frame), $P - p$ is the 4-momentum of the struck parton and $p = (p_0, \mathbf{p})$ is the total 4-momentum of all other constituents (quarks and gluons) to which we refer as the “spectator”. The vertex Γ is a sum of all possible diagrams describing the virtual nucleon disintegration into quarks and gluons, Fig. 2.

The scattering amplitude (the square block in Fig. 1) satisfies a Bethe-Salpeter equation, shown schematically in Fig. 4,

$$T = V + VG_0T, \quad (2.1)$$

where the Green’s function G_0 can be written as

$$\langle p|G_0(\mathcal{P})|p'\rangle = ig_s(p)g_0(\mathcal{P} - p)\delta(p - p'). \quad (2.2)$$

Here $g_s(p)$ is the spectator Green’s function, and $g_0(\mathcal{P} - p)$ is a Green’s function for a struck quark :

$$g_0(\mathcal{P} - p) = \frac{1}{(\mathcal{P} - p)^2 - m^2 + i\epsilon}, \quad (2.3)$$

where \mathcal{P} is the total 4-momentum of the system ($\mathcal{P} = P + q$ for the kinematics in Fig. 1) and m is the struck parton mass. The driving (interaction) term V in Eq. (2.1) is a sum of all irreducible diagrams which do not include the struck quark and the spectator in an intermediate state. Since quarks are confined at large distances, this term is singular for $(p - p')^2 \rightarrow 0$ (for instance, $\langle p|V|p'\rangle \sim (p - p')^{-4}$ in the case of linear-rising confinement).

The corresponding Bethe-Salpeter equation for the vertex function Γ is obtained from Eq. (2.1) by taking the limit $\mathcal{P}^2 \rightarrow P^2 = M^2$. Since the amplitude T factorizes near the nucleon pole

$$T(\mathcal{P}, p, p') \rightarrow \frac{\Gamma(P - p, p)\Gamma(P - p', p')}{\mathcal{P}^2 - M^2} \quad (2.4)$$

one finds the following equation

$$\Gamma = VG_0(P)\Gamma, \quad (2.5)$$

which is shown schematically in Fig. 5.

By introducing the interacting (full) Green's function

$$G = G_0 + G_0VG_0 + \dots = \frac{1}{G_0^{-1} - V} \quad (2.6)$$

we can represent the structure function $W(Q^2, \nu)$ as

$$W(Q^2, \nu) = \frac{1}{\pi} \text{Im} \int \Phi(P, p) \langle p|G(P + q)|p'\rangle \Phi(P, p') \frac{d^4p d^4p'}{(2\pi)^8}, \quad (2.7)$$

where

$$\Phi(P, p) = \frac{\Gamma(P - p, p)}{(P - p)^2 - m^2} \equiv g_0(P - p)\Gamma(P - p, p) \quad (2.8)$$

is the relativistic bound state wave function.

The IA of the structure function W corresponds to $G \rightarrow G_0$ in Eq. (2.7). This approximation can be applied if the contribution from the interaction V is small. However, this

may not be the case, in particular because of the infra-red singularity in V . The singularity can generate large corrections from the higher order terms of the expansion (2.6). Yet, it does not imply that the correction terms would remain large in any other expansions of the Green's function G . Indeed, the bound state wave function is generated by the same driving term V , Eq. (2.5), so that the singular part of V can be compensated by some part of the mass and kinetic energy terms of in the full Green's function $G = [G_0^{-1} - V]^{-1}$, when the latter is substituted into Eq. (2.7). In fact, one finds from Eqs. (2.5), (2.8) the following relation

$$[V - G_0^{-1}(P)]g_s|\Phi\rangle = 0, \quad (2.9)$$

which in nonrelativistic limit corresponds to cancellations between the binding potential and the kinetic and binding energy terms in the Schroedinger equation.

Eq. (2.9) suggests to expand the total Green's function in (2.7) in powers of the operator $h \equiv h(P) = V - G_0^{-1}(P)$ instead of the IA expansion (2.6), in powers of V . We thus obtain

$$G = \tilde{G} + \tilde{G}h\tilde{G} + \tilde{G}h\tilde{G}h\tilde{G} + \dots, \quad (2.10)$$

where $\tilde{G}^{-1} \equiv \tilde{G}^{-1}(\mathcal{P}, P) = G^{-1}(\mathcal{P}) - G^{-1}(P)$. It can be rewritten explicitly as

$$\langle p|\tilde{G}^{-1}(\mathcal{P}, P)|p'\rangle = \langle p|V(P) - V(\mathcal{P})|p'\rangle + g_s^{-1}(p)[(\mathcal{P} - p)^2 - (P - p)^2]\delta(p - p') \quad (2.11)$$

One notes that in a general, the driving term V is not local, and therefore it may depend on the total 4-momentum \mathcal{P} of the whole system (Fig. 4). However, for a local interaction, $\langle p|V(\mathcal{P})|p'\rangle \equiv V(p - p')$, so that the terms containing V in Eq. (2.11) cancel. Then

$$\langle p|\tilde{G}(\mathcal{P}, P)|p'\rangle = i g_s(p)\tilde{g}(\mathcal{P} - p, P - p)\delta(p - p'), \quad (2.12)$$

where

$$\tilde{g}(\mathcal{P} - p, P - p) = \frac{1}{(\mathcal{P} - p)^2 - (P - p)^2 + i\epsilon} \quad (2.13)$$

is a modified, quasi-free, Green's function of the struck parton with 4-momentum $\mathcal{P} - p$. Unlike the Green's function g_0 , Eq. (2.3), the modified Green's function \tilde{g} , as well as \tilde{G} ,

depends on the target 4-momentum P , which is related to the entire interacting system. The appearance of such an additional parameter is not surprising, since \tilde{g} has been designed to approximate the *interacting* Green's function. Note that the pole in \tilde{g} does not appear at the quark mass $(\mathcal{P} - p)^2 = m^2$ as in the free Green's function g_0 , but at an off-shell point, $(\mathcal{P} - p)^2 = (P - p)^2$.

Substituting Eqs. (2.10), (2.12) into Eq. (2.7) we obtain the structure function W in an expansion in powers of $\tilde{G} = g_s \tilde{g}$ for $\mathcal{P} = P + q$. Consider the limit $Q^2 \rightarrow \infty$ and $x = Q^2/2m\nu = \text{const}$. Then $\nu = Q^2/2Mx \sim Q^2$, $\nu/|\mathbf{q}| \rightarrow 1$, and

$$\begin{aligned}\tilde{g}^{-1}(P + q - p, P - p) &= (P - p + q)^2 - (P - p)^2 + i\epsilon \\ &= 2(M - p_0)\nu + 2\mathbf{p} \cdot \mathbf{q} - Q^2 + i\epsilon \sim Q^2\end{aligned}\quad (2.14)$$

Therefore Eq. (2.10) represents in fact an expansion in powers of $1/Q^2$, and

$$F = \nu W = \frac{\nu}{\pi} \text{Im} \langle \Phi | \tilde{G} + \tilde{G} h \tilde{G} + \dots | \Phi \rangle = \mathcal{F}_0 + \frac{\mathcal{F}_1}{Q^2} + \frac{\mathcal{F}_2}{Q^4} + \dots \quad (2.15)$$

Each term of this expansion can be represented by a modified Feynman diagram. Take for instance the first two terms

$$\mathcal{F}_0 = \frac{\nu}{\pi} \text{Im} \int i \frac{d^4 p}{(2\pi)^4} \frac{\Phi^2(P, p) g_s^2(p)}{(P - p + q)^2 - (P - p)^2 + i\epsilon} \quad (2.16a)$$

$$\frac{\mathcal{F}_1}{Q^2} = \frac{\nu}{\pi} \text{Im} \int i \frac{d^4 p d^4 p'}{(2\pi)^8} \frac{\Phi(P, p) g_s(p) h(P, p, p') g_s(p') \Phi(P, p')}{[(P - p + q)^2 - (P - p)^2 + i\epsilon][(P - p' + q)^2 - (P - p')^2 + i\epsilon]} \quad (2.16b)$$

One can easily see that these terms correspond to the two diagrams in Fig. 6, where the Feynman propagator $(k^2 - m^2)^{-1}$ for the struck parton with 4-momentum k is replaced by $[k^2 - (k - q)^2]^{-1}$. We mark it with “ \sim ”.

Let us consider the first order term, \mathcal{F}_1 , Eq. (2.16b), which involves the interaction V . One gets from Eqs.(2.9), (2.12)

$$h \tilde{g} g_s | \Phi \rangle = [h, \tilde{g}] g_s | \Phi \rangle = [V, \tilde{g}] g_s | \Phi \rangle \quad (2.17a)$$

$$\langle \Phi | g_s \tilde{g} h = \langle \Phi | g_s [\tilde{g}, h] = -\langle \Phi | g_s [V, \tilde{g}] \quad (2.17b)$$

Therefore Eq. (2.16b) can be rewritten as

$$\mathcal{F}_1 = \frac{\nu}{2\pi} Q^2 \text{Im } i \langle \Phi | g_s [[\tilde{g}, V], \tilde{g}] g_s | \Phi \rangle \quad (2.18)$$

where the interaction enters through the double commutator of V and the Green's function \tilde{g} . Using Eqs. (2.13), (2.14) we can write Eq. (2.18) explicitly as

$$\mathcal{F}_1 = \nu Q^2 \text{Im} \int i \frac{d^4 p d^4 p'}{(2\pi)^9} \frac{\Phi(P, p) g_s(p) (2q(p - p'))^2 V(p - p') g_s(p') \Phi(P, p')}{[2(M - p_0)\nu + 2\mathbf{p} \cdot \mathbf{q} - Q^2 + i\epsilon]^2 [2(M - p'_0)\nu + 2\mathbf{p}' \cdot \mathbf{q} - Q^2 + i\epsilon]^2} \quad (2.19)$$

Here we find the factor $(q(p - p'))^2$ in front of V , which removes the infra-red singularity, $V \sim 1/(p - p')^4$, in \mathcal{F}_1 . In fact, this factor reduces the contribution of \mathcal{F}_1 to the structure function even for a non-singular interaction, provided that the scattering amplitude of a high-momentum quark peaks in the forward direction. One can show that the same procedure removes the infra-red singularity also in higher orders in the expansion (2.15) for F . A direct evaluation of \mathcal{F}_1 for the case of a heavy spectator is given in Sec. 4, where we explicitly demonstrate that this term is small compared to \mathcal{F}_0 , even at moderate Q^2 . Now we concentrate on the first term, \mathcal{F}_0 , in the expansion (2.15).

III. THE LEADING TERM

A. New scaling variable.

Since our expansion (2.15) minimizes the first order correction term, the structure function F can be well approximated by the first term, \mathcal{F}_0 , Eq. (2.16a), which corresponds to the first graph in Fig. 6. Actually, this graph represents an infinite sum of diagrams corresponding to gluon and quark emission, Fig. 7, which results in logarithmic corrections to Bjorken scaling and has been studied in great detail [4]. Our treatment of these processes is not different from the standard approaches except for the modified propagator \tilde{g} , marked by “ \sim ” in Figs. 6, 7. Let us analyze the consequences of this modification. As an example we consider the two diagrams shown in Fig. 7. The first graph corresponds to a process

with no gluon emission. For simplicity we take the spectator quarks to be a diquark of mass m_s , thus

$$g_s(p) = \frac{1}{p^2 - m_s^2 + i\epsilon} \quad (3.1)$$

Substituting Eq. (3.1) into Eq. (2.16a) one finds

$$\mathcal{F}_0^{(0)} = \nu \int \frac{d^4 p}{(2\pi)^3} |\Phi^{(0)}(P, p)|^2 \delta(p^2 - m_s^2) \delta[(P - p + q)^2 - (P - p)^2], \quad (3.2)$$

where $\Phi^{(0)}$ is a component of the proton wave function, Eq. (2.8), with the vertex Γ replaced by $\Gamma^{(0)}$, corresponding to nucleon disintegration with no gluon emission (Fig. 2). Integrating over p_0 and neglecting the contribution from negative energy states (pair production) we get from the first δ -function: $p_0 = E_p = (m_s^2 + \mathbf{p}^2)^{1/2}$. Then using (2.14) we can rewrite Eq. (3.2) as

$$\begin{aligned} \mathcal{F}_0^{(0)} &= \nu \int \frac{d^3 p}{(2\pi)^3} |\tilde{\phi}^{(0)}(|\mathbf{p}|)|^2 \delta[(M - E_p)\nu + \mathbf{p} \cdot \mathbf{q} - Q^2/2] = \frac{\nu}{|\mathbf{q}|} \int_{|\tilde{y}|}^{\infty} \frac{pdp}{(2\pi)^2} |\tilde{\phi}^{(0)}(|\mathbf{p}|)|^2 \\ &= \frac{\nu}{|\mathbf{q}|} \int \frac{d^3 p}{(2\pi)^3} |\tilde{\phi}^{(0)}(|\mathbf{p}|)|^2 \delta(p_z + \tilde{y}), \end{aligned} \quad (3.3)$$

where $\tilde{\phi}^{(0)}(|\mathbf{p}|) = \Phi(P, E_p, \mathbf{p})/2E_p^{1/2}$. The variable \tilde{y} is the minimal momentum of the struck quark, $-\mathbf{p}_{min} = \tilde{y}\mathbf{q}/|\mathbf{q}|$, obtained from the equation

$$2 \left(M - \sqrt{\tilde{y}^2 + m_s^2} \right) \nu - 2\tilde{y}|\mathbf{q}| - Q^2 = 0. \quad (3.4)$$

The latter corresponds to energy conservation, given by the δ -function in Eq. (3.3), when the struck quark is equally off-mass shell before and after the virtual photon absorption. Solving Eq. (3.4) and using $\nu = Q^2/2Mx$, $\mathbf{q}^2 = Q^2 + \nu^2$ we obtain

$$\tilde{y}(x, Q^2)/M = \frac{(1-x)^2 - (m_s/M)^2}{\sqrt{(1-x)^2 + 4m_s^2 x^2/Q^2} + \sqrt{(1-x)^2 + 4M^2 x^2(1-x)^2/Q^2}} \quad (3.5)$$

It follows from Eq. (3.3) that $(|\mathbf{q}|/\nu)\mathcal{F}_0^{(0)} \equiv f(\tilde{y})$ is a function of the scaling variable \tilde{y} only. In the nonrelativistic limit and for zero binding energy, this variable coincides with the West scaling variable y , Eq. (1.2).

Eq. (3.2) for $\mathcal{F}_0^{(0)}$ can be rewritten in terms of light-cone variables: $p \equiv (p_+, p_-, \mathbf{p}_\perp)$, where $p_\pm = p_0 \pm p_z$. Here the negative z -axis has been chosen along the virtual photon direction, so that $q_\pm = \nu \mp |\mathbf{q}|$, and $\mathbf{q}_\perp = 0$. Introducing the light-cone fractions $z = (P_+ - p_+)/P_+$ and $\xi = -q_+/P_+$, where $P_\pm = M$ is the target light-cone momentum, and integrating over p_- , one obtains

$$\mathcal{F}_0^{(0)} = \nu \int \frac{d^2 p_\perp dz}{2(2\pi)^3} \frac{|\bar{\Phi}^{(0)}(p_\perp, z)|^2}{(1-z)(z-\xi)} \delta \left(M^2 + Mq_- - \frac{\bar{m}^2 + p_\perp^2}{z-\xi} - \frac{m_s^2 + p_\perp^2}{1-z} \right) \quad (3.6)$$

where $Mq_- = Q^2/\xi$ and

$$\bar{m}^2 = (P - p)^2 = zM^2 - \frac{zm_s^2 + p_\perp^2}{1-z} \quad (3.7)$$

The expression (3.6) for $\mathcal{F}_0^{(0)}$ clearly corresponds to the first diagram in Fig. 8, calculated according the rules of light-cone perturbation theory, where the struck quark mass equals \bar{m} . Similar to the previous calculations one finds after integration over \mathbf{p}_\perp and z in (3.6) that the structure function depends only on a single (scaling) variable \bar{x} . The latter is the value of the light-cone fraction z , corresponding to the zero of the δ -function argument in Eq. (3.6) for $p_\perp = 0$. One finds

$$\bar{x} = \frac{x + \sqrt{1 + 4M^2x^2/Q^2} - \sqrt{(1-x)^2 + 4m_s^2x^2/Q^2}}{1 + \sqrt{1 + 4M^2x^2/Q^2}} \quad (3.8)$$

Since \bar{x} corresponds to the light-cone fraction of the off-shell struck quark with 4-momentum $P - p$ (Fig. 7), where $p = (\sqrt{m_s^2 + \tilde{y}^2}, -\tilde{y}\mathbf{q}/|\mathbf{q}|)$, one can easily verify that \bar{x} is related to \tilde{y} by

$$\bar{x} = 1 - \frac{\sqrt{m_s^2 + \tilde{y}^2} + \tilde{y}}{M} \quad (3.9)$$

It is interesting to compare \bar{x} with the Nachtmann [9] scaling variable, ξ

$$\xi = \frac{2x}{1 + \sqrt{1 + 4M^2x^2/Q^2}}, \quad (3.10)$$

which corresponds to the light-cone fraction of the on-mass-shell struck parton of zero mass [10]. The denominator of this expression takes into account the kinematical target mass

corrections to the x -scaling. Similar target mass effects are accounted for in Eq. (3.8) for the scaling variable \bar{x} . It is not surprising, since no assumptions have been made for the value of the target mass M in Eqs. (3.3), (3.6). However, \bar{x} includes also dynamical corrections to the x -scaling, which are not present in the variable ξ . These are taken into account by the last term in the numerator of Eq. (3.8). It can be seen in a more pronounced way if we consider large Q^2 limit. Then using Eqs. (3.8), (3.10) one easily finds that \bar{x} and ξ -variables are related by

$$\bar{x} \simeq \xi + \frac{M^2 x^2}{Q^2} - \frac{m_s^2 x^2}{(1-x)Q^2} \quad (3.11)$$

Thus $\bar{x} \rightarrow \xi \rightarrow x$ for $Q^2 \rightarrow \infty$. However, the term $m_s^2 x^2 / (1-x)Q^2$ makes \bar{x} and ξ be quite different for finite Q^2 , in particular for high x . As an example we plot the variables ξ and \bar{x} as functions of Q^2 for $x = 0.75$ in Fig. 9, for a spectator mass $m_s = M$. One finds that \bar{x} approaches the Bjorken variable x (the dotted line) much more slowly than the Nachtmann variable ξ , and the difference between \bar{x} and ξ is appreciable even for rather large Q^2 . For small x , however, the variable \bar{x} is close to ξ or x , unless the spectator mass is not very large.

B. Gluon radiation.

Consider the second diagram in Fig. 7, which describes gluon emission. Its contribution to the structure function can be written as

$$\mathcal{F}_0^{(1)} = \nu \int \frac{d^4 p d^4 p'}{(2\pi)^8} |\Phi^{(1)}(P, p', p - p')|^2 \delta(p'^2 - m_s^2) \delta(p - p')^2 \delta[(P - p + q)^2 - (P - p)^2] \quad (3.12)$$

where $\Phi^{(1)}$ is the component of the proton wave function corresponding to the vertex $\Gamma^{(1)}$ in Fig. 2. It is related to $\Phi^{(0)}$ by

$$|\Phi^{(1)}(P, p', p - p')|^2 = \frac{4\pi\alpha_s |\Phi^{(0)}(P, p')|^2}{(p - p')^2 - m^2}, \quad (3.13)$$

where α_s is the QCD running coupling constant. After integration over the p_0 and p'_0 we can rewrite $\mathcal{F}_0^{(1)}$ in the form of Eq. (3.3):

$$\frac{|\mathbf{q}|}{\nu} \mathcal{F}_0^{(1)} = \int \frac{d^3 p d^3 p'}{(2\pi)^6} |\tilde{\phi}^{(1)}(\mathbf{p}, \mathbf{p}')|^2 \delta[p_z + \tilde{y}(m_s)]. \quad (3.14)$$

Here $\tilde{y}(m_s)$ is given by Eq. (3.5), where m_s is now the invariant mass of the diquark-gluon system: $m_s^2 = p^2$. In terms of light-cone variables (see Fig. 8) it can be written as

$$m_s^2 = m_d^2 + (1-z) \frac{(\mathbf{p}'_{\perp} - \mathbf{p}_{\perp})^2}{z' - z} + (z' - z) \frac{m_d^2 + \mathbf{p}'^2}{1 - z'} + \mathbf{p}'^2_{\perp} - \mathbf{p}_{\perp}^2, \quad (3.15)$$

where m_d is the diquark mass. Notice that $1 \geq z' \geq z$. Using Eq. (3.15) we rewrite Eq. (3.12) in terms of light-cone variables

$$\mathcal{F}_0^{(1)} = \nu \int \frac{d^2 p_{\perp} dz d^2 p'_{\perp} dz'}{4(2\pi)^6} \frac{|\bar{\Phi}^{(1)}(p_{\perp}, z, p'_{\perp}, z')|^2}{(1-z')(z'-z)(z-\xi)} \delta \left(M^2 + M_{q-} - \frac{\bar{m}^2 + p_{\perp}^2}{z-\xi} - \frac{m_s^2 + p_{\perp}^2}{1-z} \right), \quad (3.16)$$

where $\bar{m}^2 = (P - p)^2$, Eq. (3.7).

Eq. (3.16) describes the lowest order gluon emission contribution to the structure function, \mathcal{F}_0 . The total contribution of gluon emission to \mathcal{F}_0 corresponds to the sum of all ladder diagrams. It can be done using the same procedure as for instance in [11,12]. Our modification consists only of replacement of the struck quark mass m by \bar{m} , Eq. (3.7). Eventually, it will modify the evolution equation [13] by the replacement of the Bjorken scaling variable x by \bar{x} , Eq. (3.8), for m_s given by Eq. (3.15).

C. Approximation.

A considerable simplification can be achieved if we approximate m_s as an effective spectator mass depends only on external momenta. Since $z \rightarrow \bar{x} \simeq x$ and $z' \sim z$, one gets from Eq. (3.15)

$$m_s^2 \simeq m_d^2 + C(x, Q^2)(1-x) \quad (3.17)$$

In this case the off-shell mass \bar{m} of the struck quark, Eq. (3.7), becomes independent of z', \mathbf{p}'_{\perp} . This allows us to integrate over z', \mathbf{p}'_{\perp} in Eq. (3.16), thus reducing it to the form of Eq. (3.6) (or (3.3)). Finally one can sum all the ladder diagrams, $\mathcal{F}_0^{(i)}$ such that $|\bar{\Phi}^{(0)}(p_{\perp}, z)|^2$ in Eq. (3.6) is replaced by $u(p_{\perp}, z, Q^2)$, which is a probability to find a struck quark with momentum p inside the nucleon, and a spectator with any number of gluons. The latter gives rise to logarithmic corrections to scaling.

Eq. (3.17) for the invariant spectator mass looks quite appealing apart from its relation to Eq. (3.15). Indeed, $x = 1$ corresponds to elastic scattering, when no gluons are emitted. Therefore in this case the spectator is represented by a diquark. When x decreases, gluons are emitted and m_s^2 increases $\propto (1-x)$. The coefficient $C(x, Q^2)$ in Eq. (3.17) determines the rate of increase of the spectator mass with Q^2 and x . It can be found self-consistently from the evolution equation. However, when $x \sim 1$, one can take $C(x, Q^2) \simeq C(1, Q^2) \simeq \text{const}$, because of Q^2 -dependence of the spectator mass is less important than its x -dependence near the elastic threshold. Let us roughly estimate the value of C by using the Weizsäcker-Williams or “equivalent photon” approximation, utilized in Ref. [14] for derivation of the evolution equation. One finds from [14] that the light-cone fraction of the “equivalent” gluon, $z - z'$, (Fig. 8) is of order $\alpha_s \ln(Q^2/Q_0^2)$ in the region of large x . However, $\mathcal{F}_0^{(1)}/\mathcal{F}_0^{(0)}$ is also about the same order of magnitude. Then, as follows from Eq. (3.15), $C \sim \langle (\mathbf{p}'_{\perp} - \mathbf{p}_{\perp})^2 \rangle$, so that one could expect to find C on the scale of $(\text{GeV})^2$.

IV. CORRECTION TERM

Consider the first correction \mathcal{F}_1/Q^2 , Eq. (2.15), to the leading term \mathcal{F}_0 . In order to simplify the evaluation of \mathcal{F}_1 , Eq. (2.19), we take the large spectator mass limit: $m_s \gg |\mathbf{p}|$, so that $g_s \rightarrow \delta(p_0 - m_s)/2m_s$. In the same limit one gets from Eq. (3.4)

$$\tilde{y} \rightarrow y = -\frac{Q^2}{2|\mathbf{q}|} + \frac{m^* \nu}{|\mathbf{q}|} \quad (4.1)$$

where $m^* = M - m_s$, and also the Green's function \tilde{g} , Eq. (2.14), reads

$$\tilde{g} = \frac{1}{2|\mathbf{q}|(p_z + y + i\epsilon)}. \quad (4.2)$$

Then the first order correction term \mathcal{F}_1 , Eq. (2.19), becomes

$$\mathcal{F}_1 = -\mathcal{A}_1 \text{Im} \frac{1}{2\pi} \int \frac{d^3p d^3p'}{(2\pi)^6} \tilde{\phi}(\mathbf{p}) \frac{(\hat{\mathbf{q}} \cdot (\mathbf{p} - \mathbf{p}'))^2 V(\mathbf{p} - \mathbf{p}')}{(p_z + y + i\epsilon)^2 (p'_z + y + i\epsilon)^2} \tilde{\phi}(\mathbf{p}') \quad (4.3)$$

where $\hat{\mathbf{q}} = \mathbf{q}/|\mathbf{q}|$, and

$$\mathcal{A}_1 = \frac{\nu^2 Q^2}{\mathbf{q}^2 4m_s \nu} = \frac{Mx}{2m_s(1 + 4M^2x^2/Q^2)} \rightarrow \frac{Mx}{2m_s}, \quad \text{for } Q^2 \rightarrow \infty \quad (4.4)$$

It is convenient to evaluate the terms \mathcal{F}_i in (2.15) using coordinate representation. Substituting

$$\tilde{\phi}(\mathbf{p}) = \int e^{i\mathbf{p}\cdot\mathbf{r}} \phi(\mathbf{r}) d^3r, \quad V(\mathbf{p} - \mathbf{p}') = \int e^{i(\mathbf{p}-\mathbf{p}')\cdot\mathbf{r}} v(\mathbf{r}) d^3r \quad (4.5)$$

into Eqs. (3.3),(4.3) one obtains after some algebra [15] the following expressions for the two first terms of the expansion (2.15)

$$\mathcal{F}_0 = \frac{\mathcal{A}_0}{2\pi} \int_{-\infty}^{\infty} ds \exp(-iys) \int d^3r \phi(\mathbf{r} - s\hat{\mathbf{q}}) \phi(\mathbf{r}) \quad (4.6a)$$

$$\mathcal{F}_1 = i \frac{\mathcal{A}_1}{2\pi} \int_{-\infty}^{\infty} ds \exp(-iys) \int d^3r \phi(\mathbf{r} - s\hat{\mathbf{q}}) \phi(\mathbf{r}) \int_0^s d\sigma [v(\mathbf{r} - \sigma\hat{\mathbf{q}}) - v(\mathbf{r})] \quad (4.6b)$$

where $\mathcal{A}_0 = \nu/|\mathbf{q}| \rightarrow 1$ for $Q^2 \rightarrow \infty$. These expressions are of the same form (up to the coefficients \mathcal{A}_i) as the first two terms of the nonrelativistic $1/|\mathbf{q}|$ expansion of the structure function [8]. One checks that the same correspondence also holds for higher order terms \mathcal{F}_i in the expansion (2.15). Explicit analytical evaluations of the first three terms in the nonrelativistic $1/|\mathbf{q}|$ expansion [8] for the harmonic oscillator and for the square well potential can be found in [7].

Let us consider the case of the linear-rising potential, $v(r) = \gamma r$. Notice that $\gamma|\mathbf{r} - \sigma\hat{\mathbf{q}}| - \gamma|\mathbf{r}| \simeq -\gamma z\sigma/r$ for large r , and therefore the integrand in Eq. (4.6b) does not increase with r . (It reflects the elimination of the infra-red singularity in the expansion (2.15)). Using this result we perform the σ -integration in Eq. (4.6b) and then relate \mathcal{F}_1 to the zero order term \mathcal{F}_0 by

$$\mathcal{F}_1 \simeq i\gamma \frac{\mathcal{A}_1}{4\pi} \frac{\partial^2}{\partial y^2} \int_{-\infty}^{\infty} ds \exp(-iys) \int d^3r \frac{z}{r} \phi(\mathbf{r} - s\hat{\mathbf{q}}) \phi(\mathbf{r}) \simeq \frac{\gamma \mathcal{A}_1}{2r_0} \frac{\partial^3}{\partial y^3} \mathcal{F}_0(y) \quad (4.7)$$

where r_0 is some average size of the system which determines the slope of the parton momentum distribution. Approximating the structure function $\mathcal{F}_0(y)$ at small y by a Gaussian, $\mathcal{F}_0(y) \sim \exp(-r_0^2 y^2)$, and using Eq. (4.7) one obtains the estimate of the first correction term

$$\frac{\mathcal{F}_1(y)}{Q^2 \mathcal{F}_0(y)} \sim \mathcal{A}_1 \frac{y\Delta}{Q^2} \quad (4.8)$$

where $\Delta = \gamma r_0$ is of the order of the first excitation energy. It means that the correction term is indeed small, so that the approximation of the structure function by \mathcal{F}_0 should be valid also for *non-asymptotic* values of $Q^2 \gtrsim \text{few (GeV/c)}^2$.

V. COMPARISON WITH DATA

In Fig. 3 we displayed the proton structure function $F_2^p(x, Q^2)$ from BCDMC [1] and SLAC-MIT [2] experiments, as functions of Q^2 for fixed x . The solid curves correspond to the 15-parameter fit to these data taken from [3]:

$$F_2^p(x, Q^2) = A(x) \left[\frac{\ln(Q^2/\Lambda^2)}{\ln(Q_0^2/\Lambda^2)} \right]^{B(x)} \left(1 + \frac{C(x)}{Q^2} \right), \quad (5.1)$$

where $Q_0^2 = 20 \text{ GeV}^2$, $\Lambda = 250 \text{ MeV}$, and

$$A(x) = \frac{(1-x)^{2.562}}{x^{0.1011}} \sum_{\ell=0}^4 a_\ell (1-x)^\ell; \quad B(x) = 0.364 - 2.764x + \frac{0.015}{x + 0.0186}; \quad C(x) = \sum_{\ell=1}^4 c_\ell x^\ell,$$

where $\{a_\ell\} = (0.4121, -0.518, 5.967, -10.197, 4.685)$, and $\{c_\ell\} = (-1.179, 8.24, -36.36, 47.76)$.

Let us treat this fit as the actual data and display it in Fig. 10 as a function of the scaling variable \bar{x} , Eq. (3.8): $\tilde{F}_2^p(\bar{x}, Q^2) = F_2^p[x(\bar{x}, Q^2), Q^2]$ (the dashed lines). The spectator is taken to be a diquark of mass $m_s = m_d = 850 \text{ MeV}$. This value of m_d is taken from the bag model or the non-relativistic quark model, which estimate the scalar and vector diquark masses somewhere within the range of 600 to 1100 MeV [16,17]. For a comparison we also displayed in Fig. 10, the structure function $F_2^p(x, Q^2)$, Eq. (5.1), as a function of Q^2 for fixed values

of x (the solid lines). The values of Q^2 for $\bar{x} = \text{const}$ are taken within the limits of the data, i.e. $x(\bar{x}, Q^2) \leq 0.75$. Therefore the minimal values of Q^2 for $\bar{x}=0.65$ and $\bar{x}=0.7$ are smaller than the corresponding values of Q^2 for $x=0.65$ and $x=0.7$. Since the values of x and Q^2 for $\bar{x} = 0.75$ are outside the kinematical region of the BCDMC and SLAC-MIT experiments ($x(\bar{x}, Q^2) > 0.75$), the case of $x, \bar{x} = 0.75$ is not shown in Fig. 10.

One observes that \tilde{F}_2^p at constant \bar{x} exhibits considerably weaker Q^2 -dependence than the same structure function taken at constant x . It implies that the essential part of the Bjorken scaling violations, usually attributed to the logarithmic terms, is in fact $1/Q^2$ -corrections, incorporated in the scaling variable \bar{x} . In order to assess what part of the x -scaling violation is accounted for by use of the scaling variable \bar{x} , we consider the following procedure. Let us take the proton structure function, $F_2^p(\bar{x}, Q^2)$, at $Q^2 = 250 \text{ (GeV/c)}^2$, which corresponds to the largest value of Q^2 for the data sets in Fig. 3. In that region of Q^2 the scaling variable \bar{x} is very close to x , and therefore $F_2^p(x, 250) \cong \tilde{F}_2^p(x, 250)$ (see Fig. 10). The corresponding ‘‘asymptotic’’ proton structure function $f^p(x) = F_2^p(x, 250)$, obtained from the fit (5.1), is shown in Fig. 11, together with three data points for $Q^2 = 250 \text{ (GeV/c)}^2$. The dotted part corresponds to the same fit, Eq. (5.1), extended beyond the limit of the data ($x > 0.75$). The scaling of the structure function in the \bar{x} variable, $\tilde{F}_2^p(\bar{x}, Q^2) = f^p(\bar{x})$, generates the Q^2 -dependence of the same structure function taken at constant x ,

$$F_2^p(x, Q^2) = f^p[\bar{x}(x, Q^2)]. \quad (5.2)$$

Then the deviations of Eq. (5.2) from the data would explicitly show of what part of the x -scaling violations is *not* incorporated in the variable \bar{x} .

The results of this analysis are presented in Fig. 12, with $F_2^p(x, Q^2)$, Eq. (5.2), given by dashed lines. As in the previous analysis (Fig. 10) the spectator has been taken to be a diquark, $m_s = m_d = 850 \text{ MeV}$ and $C = 0$ in Eq. (3.17). One sees that the Q^2 -dependence of at $x = 0.75$ is well reproduced. The Q^2 -dependence of the other data sets is reproduced only partially, and the deviations from data increase for smaller x . However, the increase of spectator mass, m_s , as $1 - x$, Eq. (3.17), can well influence the Q^2 -dependence even in

the region of small x . The evolution of the spectator mass with x and Q^2 is given by the coefficient C in Eq. (3.17). For large x this coefficient can be taken as a constant. It then may be extracted from data by requiring that Eq. (5.2) reproduce two large x data sets, for instance $x = 0.75$ and $x = 0.65$. Since each data set is fitted by adjusting the spectator mass m_s , Eq. (3.17) fixes also the parameter m_d , which is the value of diquark mass in the elastic limit ($x = 1$). Since in this limit the nucleon is not excited, one expects m_d to be on the order of two constituent quark masses, i.e. 500 - 1000 MeV [16–18]. It appears however, that the two data sets cannot be fitted with such values of m_d , but only with $m_d \approx 0$ and $C \approx 3$ (GeV)². This corresponds to a spectator built out of very light quarks.

Taking $m_d = 0$ in Eq. (3.17), we find for the scaling variable \bar{x} , Eq. (3.8),

$$\bar{x} = \frac{x + \sqrt{1 + 4M^2x^2/Q^2} - \sqrt{(1-x)^2 + 4C(1-x)x^2/Q^2}}{1 + \sqrt{1 + 4M^2x^2/Q^2}} \quad (5.3)$$

One gets from Eq. (5.3) that $\bar{x} = 1$ for $x = 1$, so that the two scaling variables vary within the same limits.

Proton structure function given by Eqs. (5.2), (5.3) for $C = 3$ is shown in Fig. 13 by dashed lines. Rather good agreement with the data is observed even for $x < 0.65$, although one expects large logarithmic corrections in this region and also the variation of C should be taken into account when x is far from 1. It is therefore of greater interest to make a comparison for $x > 0.75$. We show in Fig. 14a the data for the proton structure function taken from new SLAC measurements in the threshold region for $7 < Q^2 < 30$ (GeV/c)² [19], together with three high-statistics spectra for $Q^2=5.9, 7.9, \text{ and } 9.8$ (GeV/c)² from a previous SLAC experiment [20]. These data do not scale either in the variable x (Fig. 14a), or in the Nachtmann variable ξ [19]. In contrast, excellent scaling (Fig. 14b) is observed when the data are plotted as a function of \bar{x} , Eq. (5.3), with $C=3$. It is even more remarkable that the structure function obtained from these data completely coincides with the asymptotic structure function $f^p(x) = F_2^p(x, 250)$ taken from BCDMC experiment (Fig. 11) and shown by the solid line. This confirms the dominance of the quasi-free term \mathcal{F}_0 , Eq. (2.15), which is in line with our estimates in the previous Section. Indeed, the lowest correction term, \mathcal{F}_1 ,

is proportional to y , Eq. (4.8). Since $y = 0$ for $x = 1$ and $m_s = 0$, Eq. (3.5), it follows that $\mathcal{F}_1 \rightarrow 0$ near the elastic threshold.

The analysis of the large x data [19,20] (Fig. 14b) allows us to extract the asymptotic structure function $f^p(\bar{x}) = \tilde{F}_2^p(\bar{x}, Q^2)$, up to $x \lesssim 0.95$. We find that $f^p(\bar{x})$ is clearly below the dashed curve for $x \gtrsim 0.8$, which is the fit (5.1), extended outside the data, Fig. 11. It means that the fit (5.1) is not applicable in that region. It was shown by Drell, Yan, and West [21,22] that the threshold ($x \rightarrow 1$) behaviour of the asymptotic structure function is correlated with the large Q^2 behaviour of the elastic form factor. Using quark counting arguments one obtains $f^p(x) \sim (1-x)^3$. However additional QCD effects may effectively increase the value of the exponent [23]. This predictions can be checked by a comparison with the structure function that we extracted from the data. We find that it well described by $f^p(x) = 1.5(1-x)^{3.7}$ for $x \gtrsim 0.75$ (the dot-dashed curve in Fig. 14b).

With the asymptotic structure function $f^p(\bar{x})$, extracted from the experiment [1,19,20], we can predict the structure function at large values of x from moderate up to very high values of Q^2 . The results are shown in Fig. 15. The dashed lines correspond to Eq. (5.2), with the asymptotic structure function $f^p(x)$ given by the fit (5.1) for $x \leq .78$, $Q^2 = 250$ (GeV/c)², and $f^p(x) = 1.5(1-x)^{3.7}$ for $x \geq 0.78$. We plot also a few available data points, taken from old SLAC-MIT measurements [24], for $x = 0.78, 0.82$ and 0.86 . Again our predictions are in full agreement with the data. Still a check of our predictions for higher Q^2 would be of greater interest, since we predict a significant non-logarithmic Q^2 -dependence for large x , Fig. 15. In fact, as follows from our analysis, none of the *large x* data ($x \gtrsim 0.5$) exhibit any substantial deviations from the \bar{x} -scaling. Therefore, measurements for high Q^2 would be extremely important in order to establish the importance of logarithmic corrections in the large x region.

VI. SUMMARY

In this paper we concentrated on effects of confinement in deep inelastic scattering. Using the framework of the Bethe-Salpeter equation, we found a new expansion of the structure function in powers of $1/Q^2$ that is free of infra-red singularities and diminishes corrections to the zero-order term. The zero-order term describes scattering off a free off-mass-shell parton, which keeps the same off-shell mass in the final state. We evaluated corrections from higher order terms for the case of a linear-rising confining potential, and found them small even for rather low values of Q^2 . It allows us to consider the zero order (quasi-free) term as a good approximation for the structure function, valid in the entire Q^2 region.

By analyzing the quasi-free term we found it depends on the scaling variable \bar{x} . This variable coincides with the Bjorken variable x in the limit $Q^2 \rightarrow \infty$. However, at finite Q^2 the variables x and \bar{x} are quite different: $x - \bar{x} \sim m_s^2/(1-x)Q^2$, where m_s is the invariant mass of the spectator particles. It implies that $1/Q^2$ corrections to the x scaling would be much larger than those obtained in perturbative calculations, especially in the region of large x . These corrections could be very appreciable also at small x , since the spectator mass increases with $(1-x)$ due to gluons emission. However the evaluation of the spectator mass at small x depends on knowledge of its Q^2 -dependence, which can be obtained by using the evolution equation. In this paper we limited our analysis to the large x region, where the Q^2 -dependence of the spectator mass m_s is less important.

Using simple arguments we showed that $m_s^2 = m_d^2 + C(1-x)$ for $x \lesssim 1$. Here m_d is the diquark mass, since there is no gluon emission at the elastic threshold. First we analysed the data for the proton structure function by taking for m_d values between 500-1000 MeV, i.e., on the order of two constituent quark masses, and taking $C = 0$. Even though we found that scaling in \bar{x} is certainly better than that in x , the scaling deviations are still considerable, especially when \bar{x} approaches the elastic threshold. Next we included the gluon emission contribution to the spectator mass by taking $C \neq 0$. However, instead of taking for the diquark mass, m_d , the values from constituent quark models, we considered the nucleon

structure function data as a source of information for the value of m_d . We found that *all* large x data ($x \gtrsim 0.5$) display perfect scaling in the \bar{x} -variable for $C \approx 3$ and $m_d \approx 0$, which corresponds to very light quarks.

Since $\bar{x} \rightarrow x$ for $Q^2 \rightarrow \infty$, the perfect scaling in the \bar{x} -variable allows us to arrive at the Bjorken limit already at moderate values of Q^2 . Thus our analysis of the proton structure function near elastic threshold shows that $F_2 \sim (1-x)^{3.7}$ for $x \rightarrow 1$. This is different from the theoretical results based on simple quark counting arguments, which predict $F_2 \sim (1-x)^3$.

Untill now the measurements of the structure function for large values of x ($x > 0.75$) have not been extended beyond $Q^2 \sim 25$ (GeV/c)². The present large x data are in full agreement with our predictions based on \bar{x} -scaling, and thus do not display any noticeable effects of logarithmic terms. It would be very interesting to extend the measurements to higher values of Q^2 . The \bar{x} -scaling predicts a distinctive Q^2 -dependence in the structure function $F(x, Q^2)$ at large fixed values of the Bjorken variable x . Hence, the deviations from our predictions would establish the magnitude of the logarithmic scaling violations at large x .

VII. ACKNOWLEDGMENTS

I am grateful to A. Goldhaber and V. Zakharov for useful discussions. Special thanks to A. Rinat and B. Svetitsky for reading the manuscript and making valuable comments on it.

REFERENCES

- [1] BCDMS Collab., A.C. Benvenuti *et al.*, Phys. Lett. **B223**, 485 (1989).
- [2] A. Bodek *et al.*, Phys. Rev. **D20**, 1471 (1979).
- [3] NMC Collab., P. Amaudruz *et al.*, Phys. Lett. **B295**, 159 (1992).
- [4] R.G. Roberts, *The Structure of the Proton* (Cambridge University Press, Cambridge, UK, 1990), and references therein.
- [5] O.W. Greenberg, Phys. Rev. **D47**, 331 (1993).
- [6] G.B. West, Phys. Rep. **C18**, 264 (1975).
- [7] S.A. Gurvitz and A.S. Rinat, Phys. Rev. **C47**, 2901 (1993).
- [8] H.A. Gersch, L.J. Rodriguez and P.N. Smith, Phys. Rev. **A5**, 1547 (1972).
- [9] O. Nachtmann, Nucl. Phys. **B63**, 237 (1973); **B78**, 455 (1974).
- [10] B.L. Ioffe, V.A. Khoze and L.N. Lipatov, *Hard Processes.* , (North-Holland Physics Publishing, 1984).
- [11] A.M. Polyakov, Sov. Phys. - JETP, **34**, 1177 (1972).
- [12] Yu. L. Dokshitzer, D.L. Dyakonov, and S.I. Troyan, Phys. Rep. **58**, 269 (1980).
- [13] G. Altarelli and G. Parisi, Nucl. Phys. **B126**, 298 (1977).
- [14] R.L. Jaffe, in *Los Alamos School on Relativistic Dynamics and Quark-Nuclear Physics*, ed. M.B. Jackson and A. Picklesimer. (John Wiley and Sons, New York, 1985).
- [15] A.S. Rinat and R. Rosenfelder, Phys. Lett. **B193**, 411 (1987).
- [16] F.E. Close and A.W. Thomas, Phys. Lett. **B212**, 227 (1988).
- [17] A.W. Schreiber, A.I. Signal and A.W. Thomas, Phys. Rev. **D44**, 2653 (1991).
- [18] W. Melnitchouk, A.W. Schreiber and A.W. Thomas, Phys. Rev. **D49**, 1183 (1994).

- [19] P.E. Bosted *et al.*, Phys. Rev. D**49**, 3091 (1994).
- [20] S.E. Rock *et al.*, Phys. Rev. D**46**, 24 (1992).
- [21] S.D. Drell and T.M. Yan, Phys. Rev. Lett. **24**, 181 (1970).
- [22] G.B. West, Phys. Rev. Lett. **24**, 1206 (1970).
- [23] S.J. Brodsky, in *Lectures on Lepton Nucleon Scattering and Quantum Chromodynamics*, Vol. 4 of Progress in Physics, edited by A. Jaffe and D. Ruelle (Birkhauser, Boston, 1982).
- [24] W.B. Atwood, in *Lectures on Lepton Nucleon Scattering and Quantum Chromodynamics*, Vol. 4 of Progress in Physics, edited by A. Jaffe and D. Ruelle (Birkhauser, Boston, 1982).

FIGURES

FIG. 1. Nucleon structure function given by the imaginary part of the forward Compton amplitude. The first diagram is the Impulse Approximation, and the second one describes the Final State Interaction. The shaded area includes spectator particles (quarks and gluons).

FIG. 2. Nucleon vertex function, which describes quark and gluon emission. Quarks are shown by solid lines and gluons by wavy lines.

FIG. 3. Proton structure function from BCDMS [1] and SLAC-MIT [2] experiments. The solid curves correspond to a 15 parameter fit to these data, taken from [3].

FIG. 4. Bethe-Salpeter equation for the operator T describing interactions between the struck parton and the spectator partons in the final state.

FIG. 5. Bethe-Salpeter equation for the vertex Γ describing the relativistic bound state.

FIG. 6. Diagrammatic representation of the first two terms of the expansion (2.15). Modified propagator of the struck parton is marked by “ \sim ”.

FIG. 7. Diagrammatic representation of the leading term. Quarks and gluons are shown by solid and wavy lines respectively. The modified propagators are marked by “ \sim ”.

FIG. 8. The same as in Fig. 7, but using light-cone variables. The negative z -axis has been chosen along \mathbf{q} .

FIG. 9. Comparison between the scaling variable $\bar{x} \equiv \bar{x}(x, Q^2)$ and the Nachtmann variable $\xi \equiv \xi(x, Q^2)$, Eqs. (3.8), (3.10) for $x = 0.75$. The spectator mass equals the nucleon mass. The dotted line corresponds to $x=0.75$.

FIG. 10. The proton structure function plotted as a function of Q^2 for fixed values of the Bjorken variable x (solid lines) and the scaling variable \bar{x} , Eq. (3.8) (dashed lines).

FIG. 11. Proton structure function in the asymptotic region, $f^p(x) = F_2^p(x, 250)$, given by the fit, Eq. (5.1). Three data points are taken from [1]. The dashed part of the curve lies in the region outside the data [1].

FIG. 12. Q^2 -dependence of the structure function $F_2^p(x, Q^2)$, which corresponds to scaling in the variable \bar{x} , Eq. (5.2). The spectator is taken to be a diquark of mass $m_s = m_d = 850$ MeV.

FIG. 13. The same as in Fig. 12, but where the spectator mass is a function of x , Eq. (3.17), for $m_d = 0$ and $C = 3$ (GeV)².

FIG. 14. The structure function in the region of large x for $7 < Q^2 < 30$ (GeV/c)² [19,20], plotted (a) as a function of the scaling variable x and (b) as a function of the scaling variable \bar{x} , Eq. (5.3). Three high-statistics data sets [20] for $Q^2 = 5.9, 7.9, \text{ and } 9.8$ (GeV/c)² are marked by “+”, “x”, and “#” respectively. The solid curve and the dashed curves correspond to the asymptotic structure function, shown in Fig. 11. The dot-dashed curve in (b) corresponds to $\tilde{F}_2^p(\bar{x}, Q^2) = 1.5(1 - \bar{x})^{3.7}$.

FIG. 15. Predictions for the structure function $F_2^p(x, Q^2)$ in the region of large x . The data points [24] correspond to $x = 0.78$ (+), 0.82 (x), 0.86 (#).

$$W(Q^2, \nu) = \frac{1}{\pi} \text{Im} \left[\begin{array}{c} \text{Diagram 1} \\ + \\ \text{Diagram 2} \end{array} \right]$$

The figure shows two diagrams enclosed in large square brackets. The first diagram (left) is a trapezoidal loop with a shaded bottom arc. The bottom arc is labeled p . The left and right vertical sides are labeled $P-p$. The top horizontal side is labeled $P-p+q$. Dashed lines extend from the top corners, labeled q . The bottom corners are labeled P and Γ . The second diagram (right) is similar but includes a shaded rectangular box labeled T on the top horizontal side. The right vertical side is labeled $P-p'$. The bottom right corner is labeled Γ and p' . The bottom left corner is labeled P and Γ . The top horizontal side is labeled $P-p+q$. Dashed lines extend from the top corners, labeled q .

Fig. 1

$$\Gamma = \Gamma^{(0)} + \Gamma^{(1)} + \Gamma^{(2)} + \dots$$

The figure shows a series of diagrams representing a sum. On the left is a diagram labeled Γ consisting of a thick black horizontal bar, a gray shaded wedge, and a diagonal line. This is followed by an equals sign and a series of terms: $\Gamma^{(0)}$, $\Gamma^{(1)}$, $\Gamma^{(2)}$, and an ellipsis. Each term $\Gamma^{(n)}$ consists of a thick black horizontal bar and a diagonal line. $\Gamma^{(0)}$ has a gray shaded wedge. $\Gamma^{(1)}$ has a wavy line. $\Gamma^{(2)}$ has two wavy lines.

Fig. 2

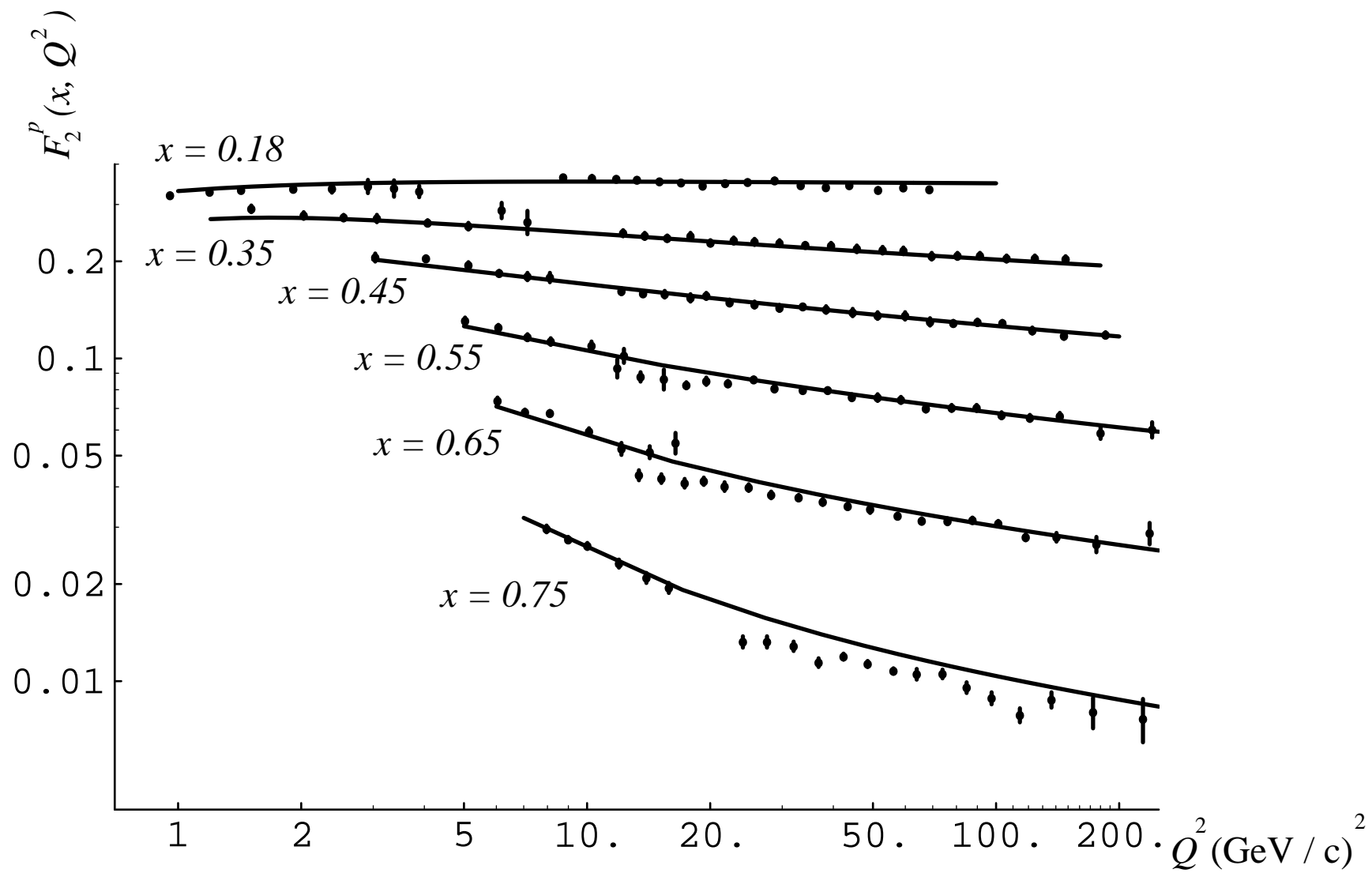


Fig. 3

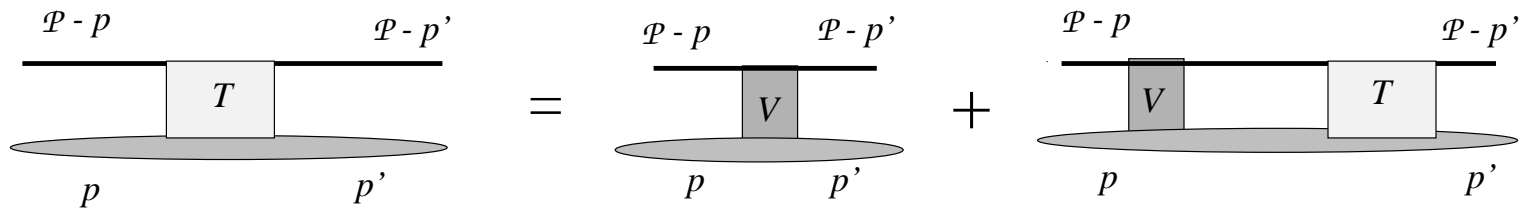


Fig. 4

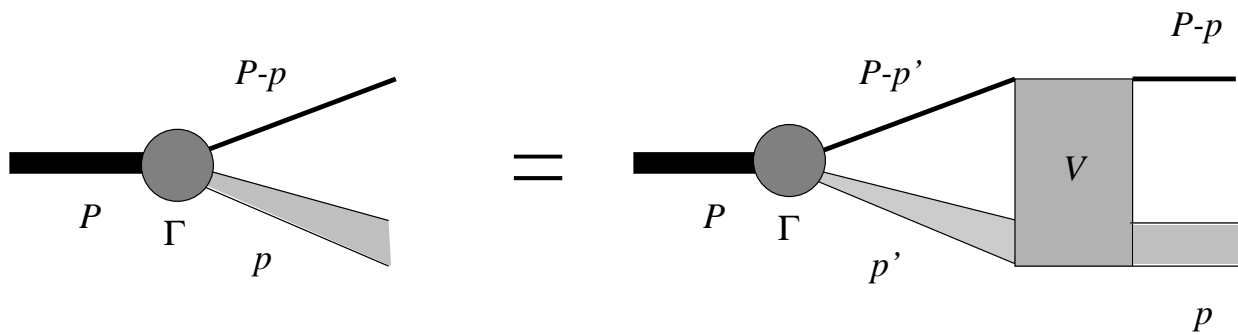


Fig. 5

$$W(Q^2, \nu) = \frac{1}{\pi} \text{Im} \left[\begin{array}{c} \text{Diagram 1} + \text{Diagram 2} + \dots \end{array} \right]$$

The diagram shows two Feynman diagrams for the imaginary part of the transition amplitude $W(Q^2, \nu)$. Both diagrams have external momenta P and Γ at the bottom vertices, and q at the top vertices. The top horizontal line has two vertices with momenta $P-p+q$ and $P-p$ (left) or $P-p+q$ and $P-p'$ (right). The bottom horizontal line has two vertices with momenta p and Γ (left) or p' and Γ (right). In the first diagram, the bottom line is a shaded oval labeled p . In the second diagram, the bottom line is a shaded oval labeled p' with a shaded rectangular region labeled h on top.

Fig. 6

$$\mathcal{F}_0 = \frac{\nu}{\pi} \text{Im} \left[\begin{array}{c} \text{Diagram 1} + \text{Diagram 2} + \dots \end{array} \right]$$

The diagram shows two Feynman diagrams for the imaginary part of the transition amplitude \mathcal{F}_0 . Both diagrams have external momenta P at the bottom vertices, and q at the top vertices. The top horizontal line has two vertices with momenta $P-p+q$ and $P-p$ (left) or $P-p+q$ and $P-p$ (right). The bottom horizontal line has two vertices with momenta p and P (left) or p' and P (right). In the first diagram, the bottom line is a solid line labeled p . In the second diagram, the bottom line is a solid line labeled p' with a wavy internal line labeled $p-p'$ connecting two vertices on the bottom line.

Fig. 7

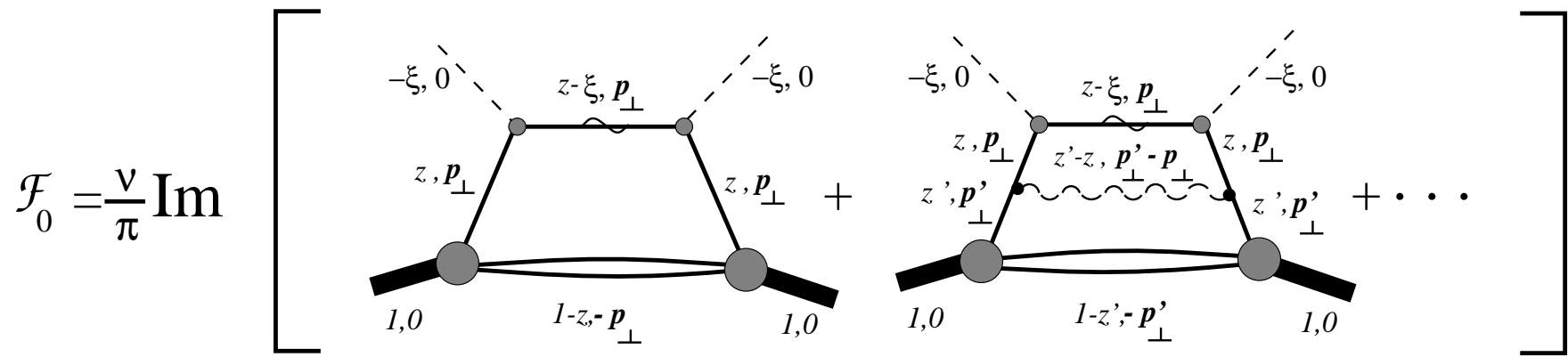


Fig. 8

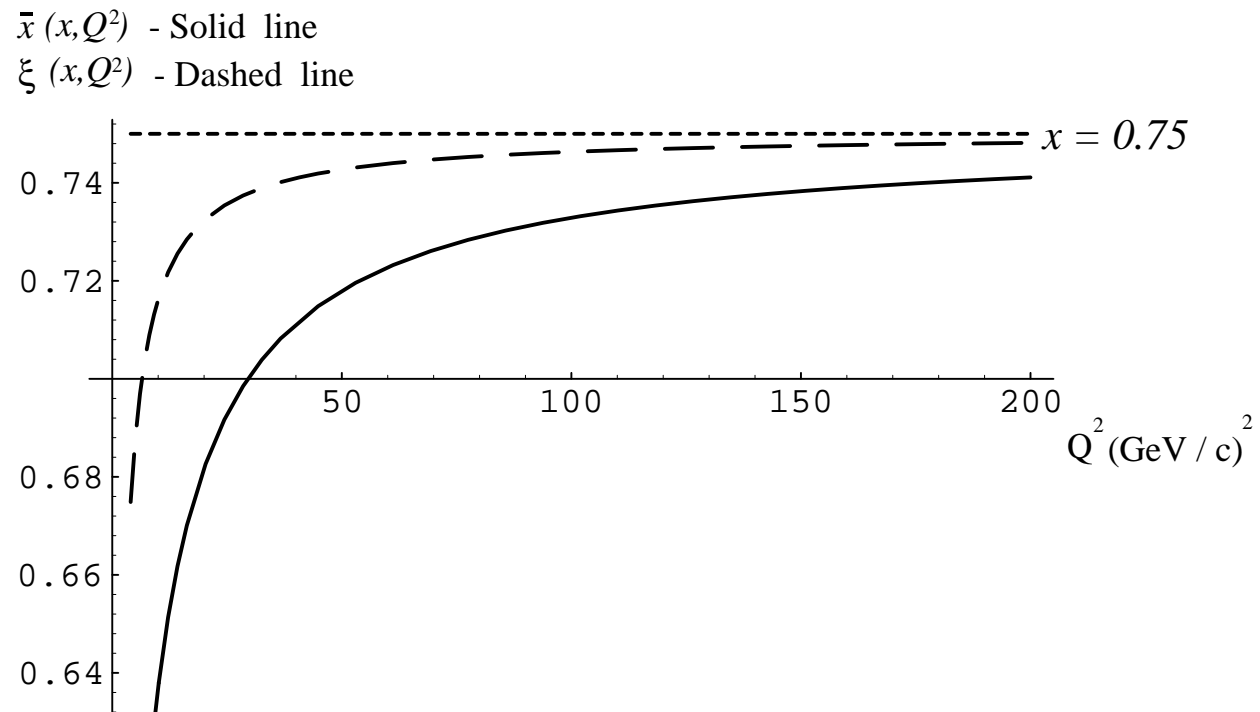


Fig. 9

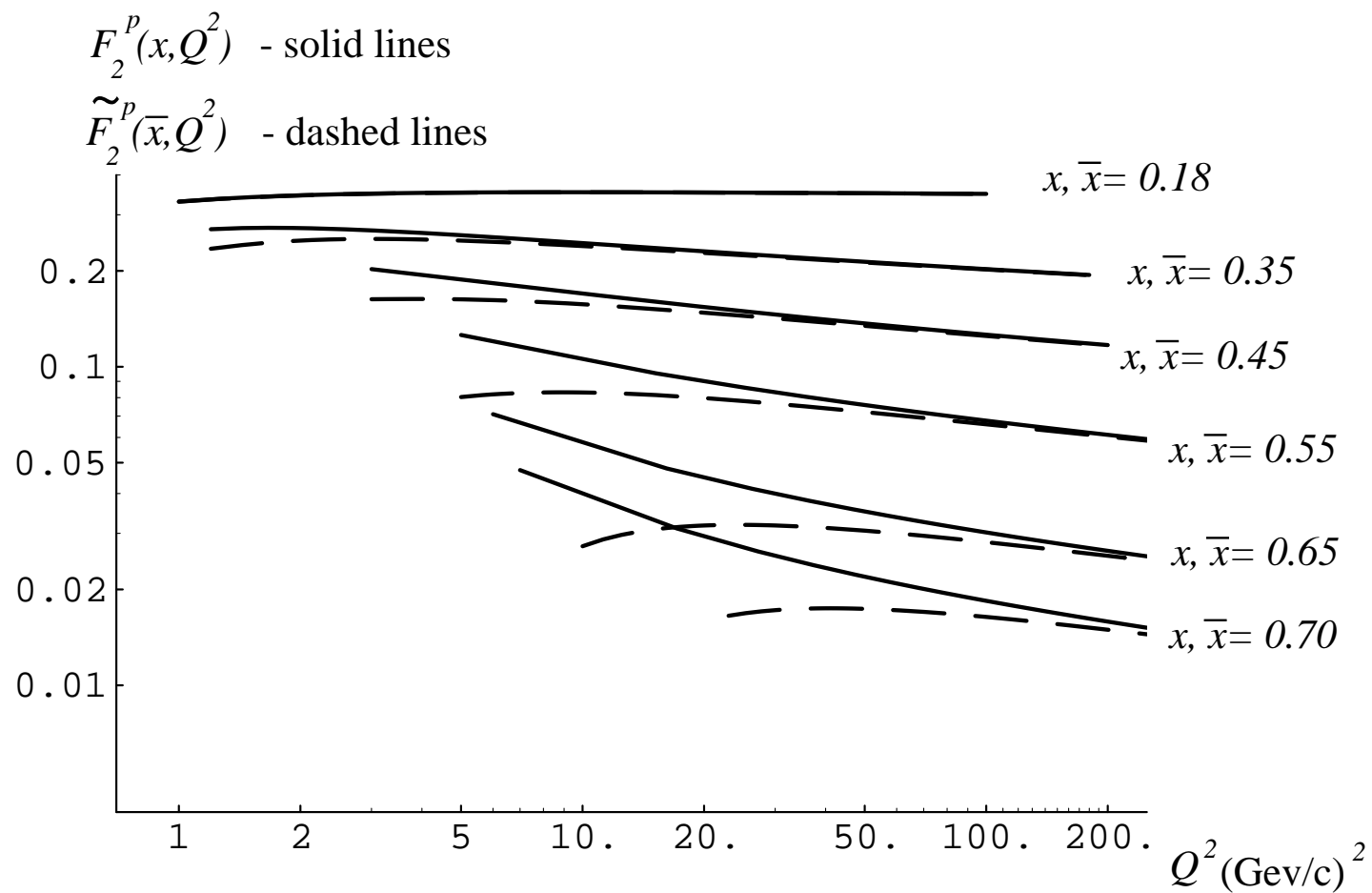


Fig. 10

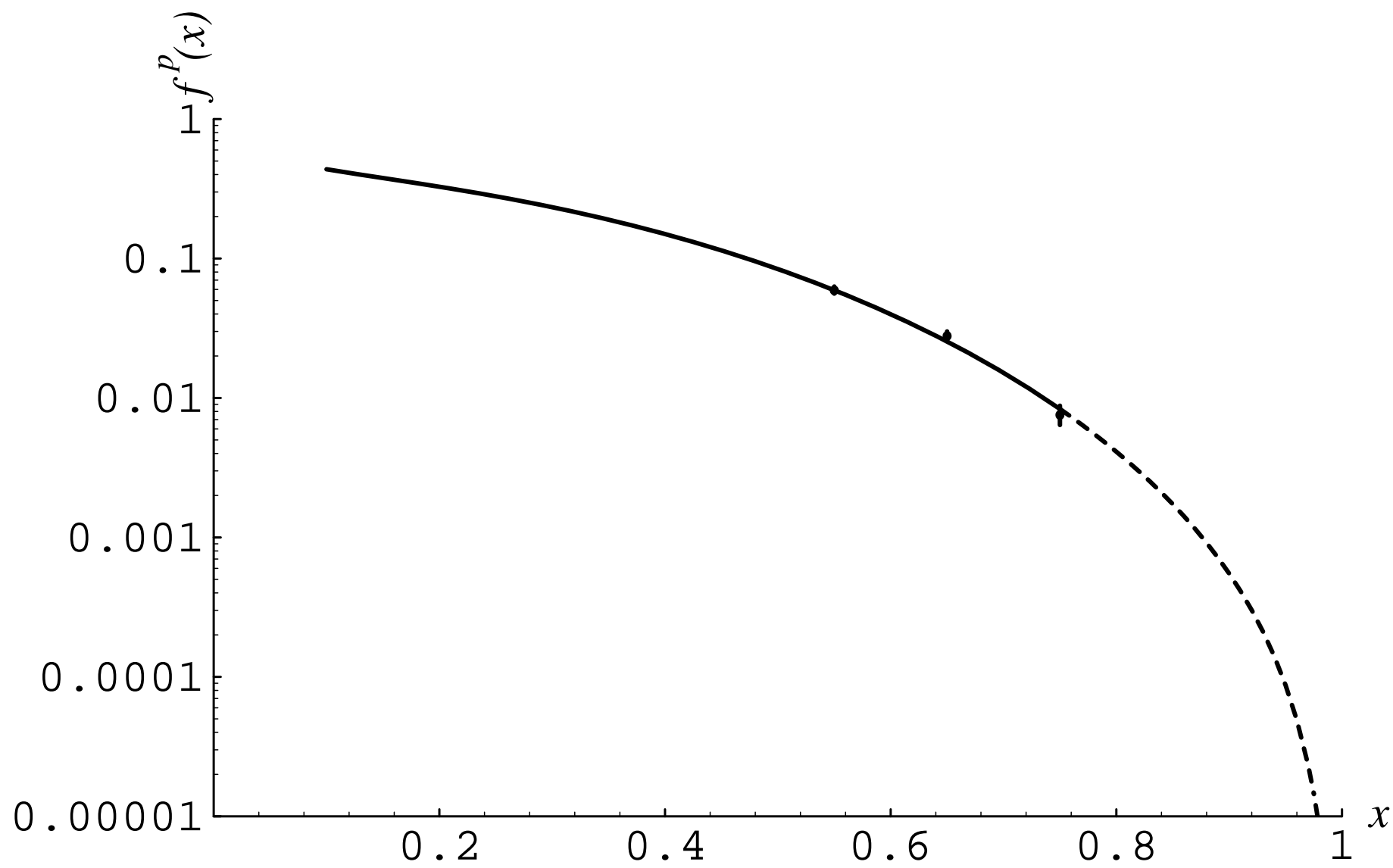


Fig. 11

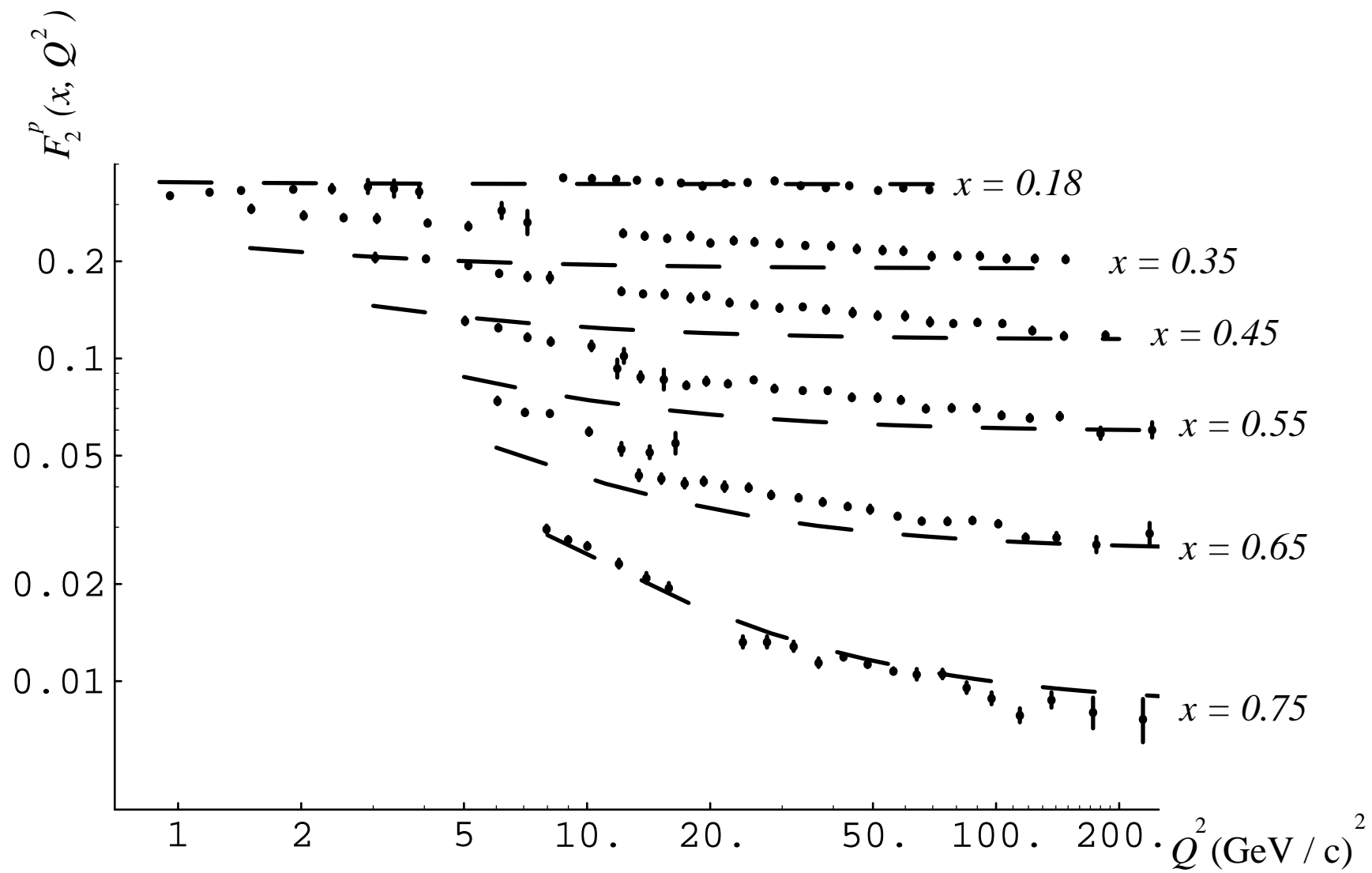


Fig. 12

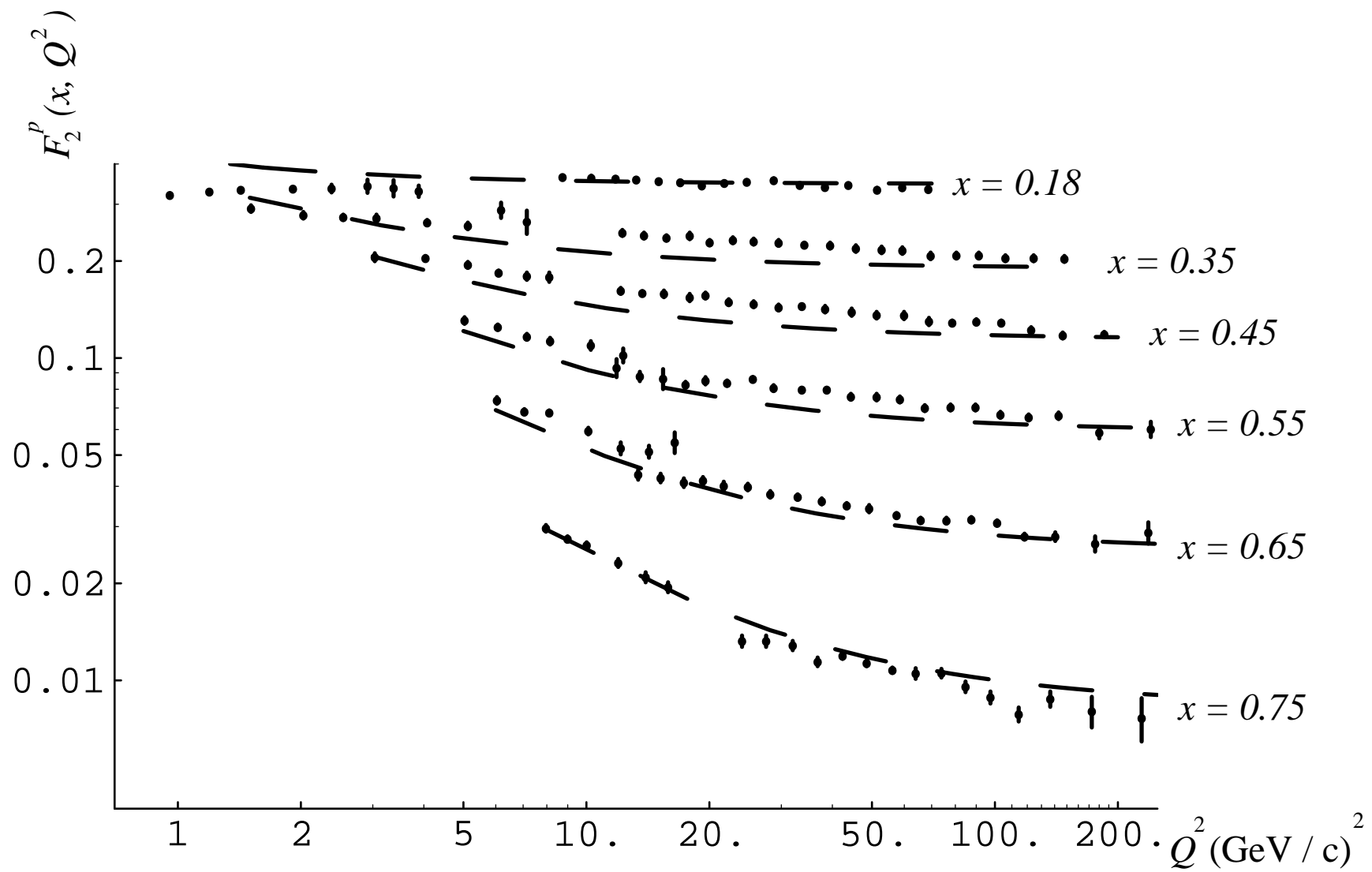


Fig. 13

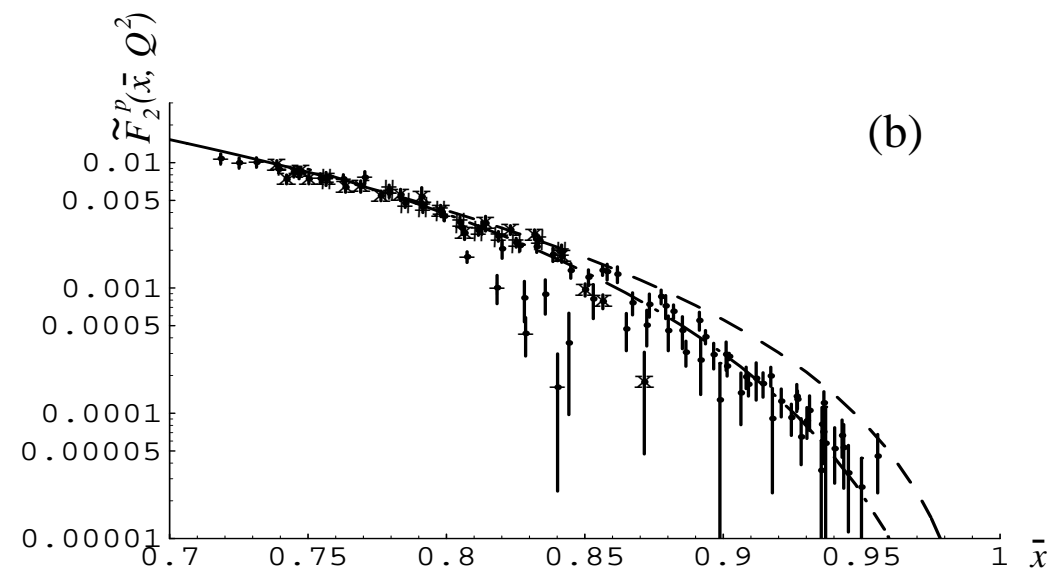
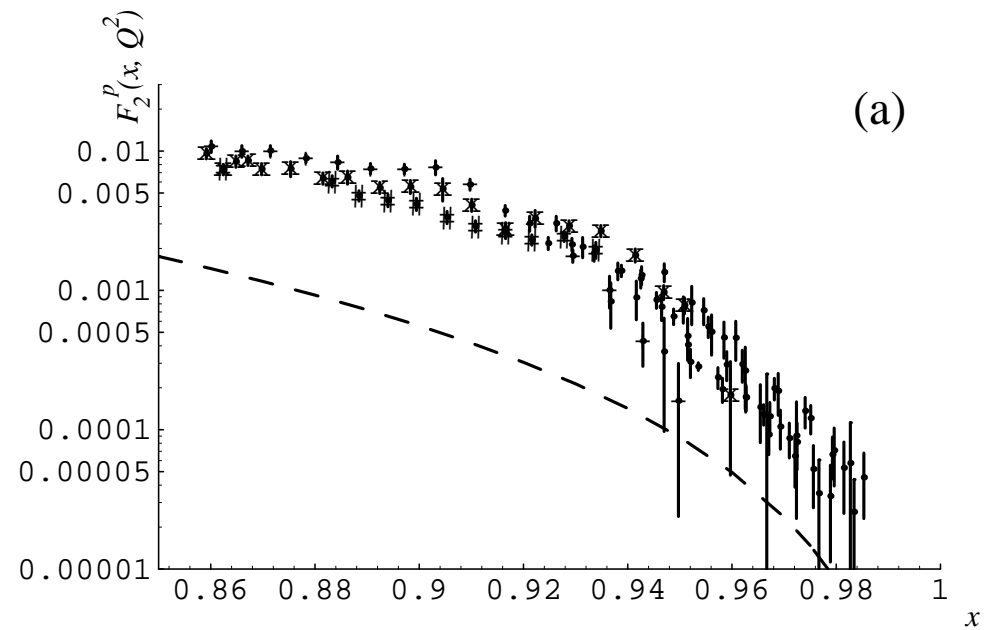


Fig. 14

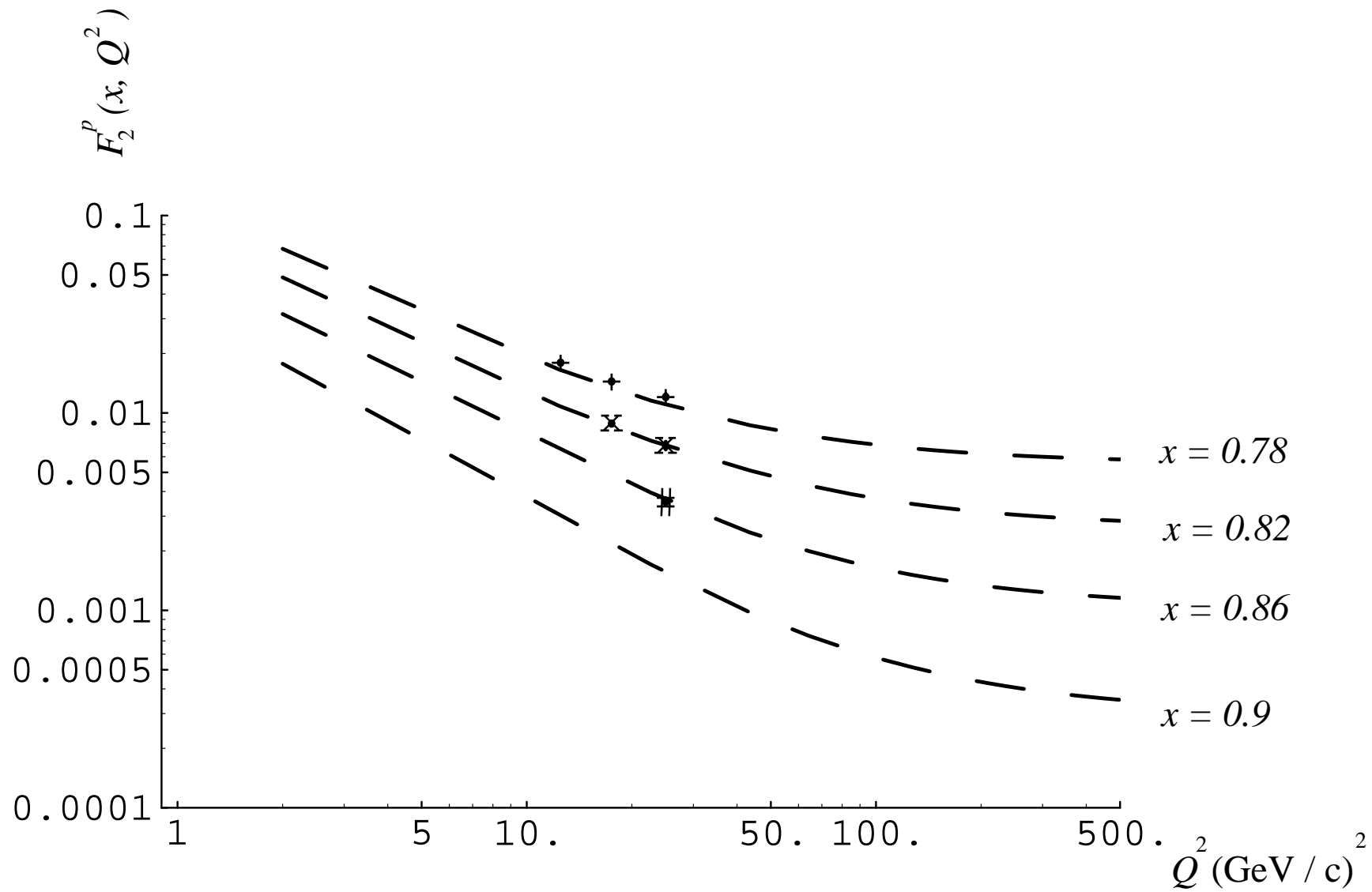


Fig. 15